Mobile Doppler Radar Observations of a Tornado in a Supercell near Bassett, Nebraska, on 5 June 1999. Part II: Tornado-Vortex Structure

HOWARD B. BLUESTEIN

School of Meteorology, University of Oklahoma, Norman, Oklahoma

WEN-CHAU LEE AND MICHAEL BELL

Atmospheric Technology Division, National Center for Atmospheric Research, Boulder, Colorado*

CHRISTOPHER C. WEISS

School of Meteorology, University of Oklahoma, Norman, Oklahoma

ANDREW L. PAZMANY

Microwave Remote Sensing Laboratory, Department of Computer and Electrical Engineering, University of Massachusetts—Amherst, Amherst, Massachusetts

(Manuscript received 18 November 2002, in final form 15 May 2003)

ABSTRACT

This is Part II of a paper detailing an analysis of high-resolution wind and reflectivity data collected by a mobile, W-band Doppler radar; the analysis depicts the near-surface life history of a tornado in a supercell in north-central Nebraska on 5 June 1999. The structure of the tornado vortex near the ground is described from a sequence of sector scans at 10–15-s intervals during much of the lifetime of the tornado. The formation of the tornado vortex near the ground is described in Part I.

The wind and reflectivity features in the tornado evolved on timescales of 10 s or less. A time history of the azimuthally averaged azimuthal and radial wind profiles and the asymmetric components of the azimuthal and radial wind fields in the tornado were estimated by applying the ground-based velocity track display (GBVTD) technique to the Doppler wind data. If the magnitude of the asymmetric part of the radial wind component were indeed much less than that of the azimuthal wind component (a necessary requirement for application of the GBVTD technique), then the azimuthal wind field was dominated by quasi-stationary wavenumber-2 disturbances for most of the lifetime of the tornado. The radius of maximum wind (RMW) contracted as the tornado intensified and increased as the tornado dissipated. Shorter-timescale oscillations in azimuthal wind speed and RMW were found that could be manifestations of inertial oscillations. Evidence was also found that the tornado vortex was two-celled when it was most intense. During the ''shrinking stage,'' the vortex remained relatively wide and intense, even though the condensation funnel had narrowed substantially.

1. Introduction

Our knowledge of the structure of tornado vortices is limited to a large extent by our restricted ability to probe tornadoes near the ground, where they are most intense and where damage is inflicted, and at high enough resolution so that their detailed structure can be resolved. In the first part of this paper (Bluestein et al. 2003, hereafter Part I), the advantages of using mobile Doppler radars at close range to map the wind field in tornadoes were identified and discussed.

A summary of what we know about tornado dynamics can be found in Davies-Jones et al. (2001). It is thought that much of the nature of the wind field in a tornado is controlled by the swirl ratio and surface friction. There are relatively few detailed analyses of the wind field in actual tornadoes. The least well understood and/or observationally verified characteristics of tornadoes are their near-surface structure and the nature of axisymmetric vertical circulations about their center.

Ground-based, portable, and mobile, X-band (3-cm wavelength) Doppler radars have been used in the last decade to determine the characteristics of the wind field

* The National Center for Atmospheric Research is sponsored by the National Science Foundation.

Corresponding author address: Dr. Howard B. Bluestein, School of Meteorology, University of Oklahoma, 100 E. Boyd, Rm. 1310, Norman, OK 73019.
E-mail: hblue@ou.edu

in tornadoes relatively near the ground, below 250 m AGL (Bluestein et al. 1993, 1997b; Bluestein 1999; Wurman and Gill 2000; Wurman 2002). Doppler radars with antennas having half-power beamwidths around 1° have achieved resolution on the order of 100 m, which is good enough to resolve structure in the subtornado-scale wind field in large tornadoes more than a kilometer across.

Bluestein et al. (1997a), using a mobile, van-mounted, W-band (3-mm wavelength/95.04 GHz) Doppler radar whose antenna had a half-power beamwidth of 0.7°, found 500-m-scale vortices along the rear-flank downdraft gust front of a nontornadic supercell. On 5 June 1999, a group from the University of Oklahoma (OU), in collaboration with a group from the Microwave Remote Sensing Laboratory (MIRSL) at the University of Massachusetts—Amherst (UMass), collected a high-resolution dataset that documented the near-surface structure of a tornado in a supercell in north-central Nebraska. The OU group used an updated version of the UMass mobile, W-band Doppler radar system, whose earlier version had been described by Bluestein et al. (1995, 1997a). In 1999 the radar was mounted on a small pickup truck and a higher-resolution antenna was installed (Bluestein and Pazmany 2000). During the 1999 spring field program, the antenna half-power beamwidth was 0.18°, thus affording a 10-m cross-beam direction resolution at 3.2-km range. Along-the-beam resolution was 15 m. The reader is referred to Part I for more information about the W-band radar system and data processing, the storm environment, and the parent storm. The purpose of this paper is to describe the tornado-vortex structure when it was mature using data from the UMass W-band radar. A description of tornadogenesis near the surface is found in Part I.

The overall life history of the tornado is given in section 2. Section 3 contains an analysis of the Doppler wind data using the ground-based velocity track display (GBVTD) technique. The structure of the tornado vortex is detailed in section 4. Section 5 is a discussion of the accuracy of the GBVTD technique. A summary of our findings, a discussion that places our results into the context of other studies, and suggestions for future work to tackle unresolved issues are found in section 6.

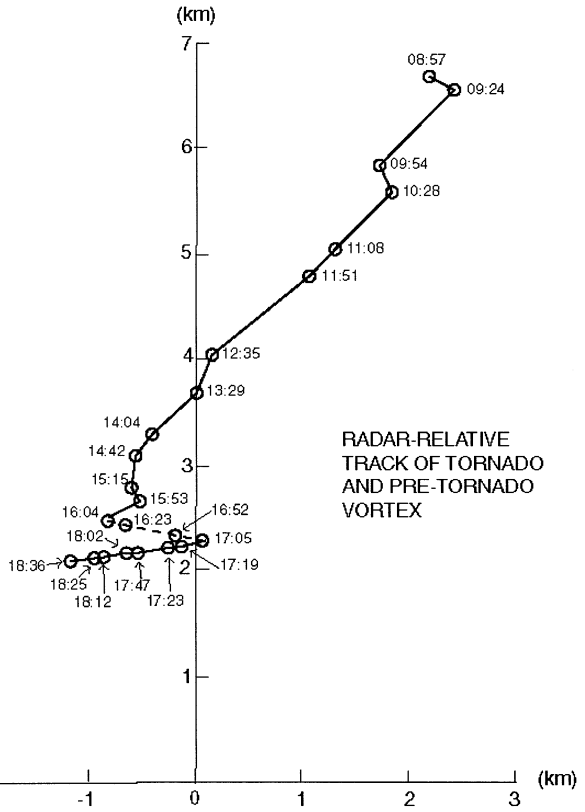

FIG. 1. Approximate track of the tornado and its precursor vortex/vorticity maximum, relative to the UMass W-band radar, which is located at the origin. Times are plotted in CDT as 20XX:YY, where XX is given in min and YY is given in s. At 2008:57, the location of the cusp in radar reflectivity is plotted. Subsequently, locations were determined subjectively from vortex signatures in the Doppler velocity and from reflectivity weak-echo holes or swirls. From prior to 2008:57, until approximately 2016:04, the radar was stationary, just east of Long Pine, NE (cf. Fig. 4 in Part I); between approximately 2016:04 and 2017:05, the radar was moving eastward along U.S. Highway 20; between approximately 2017:05 and 2018:36, the radar was stationary, just west of Bassett, NE (cf. Fig. 4 in Part I).

2. Overall life history of the tornado vortex

The track of the features associated with the tornado (Fig. 1) illustrates the location of the tornado vortex and its precursor vortex with respect to the radar. The track of the vortex signature associated with the tornado and its precursor vortex was determined subjectively by locating the approximate centers of single-Doppler cyclonic vortex signatures (Brown and Wood 1991) and echo-weak or echo-free holes or swirls in the reflectivity field, when present. The track of the tornado vortex and its precursor signature exhibits temporal and spatial continuity with the cusp/kink in the radar echo prior to 2008:57 CDT (not shown) (all times are given in CDT; UTC is 5 h later), which had been moving toward the east-northeast. The track of the vortex signature was to the northeast, approximately 30° to the left of the track of the earlier radar-echo kink; after 2014:42, the track of the vortex signature wobbled slightly. Before 2016:04, the range of the vortex signature to the radar decreased monotonically with time.

Prior to 2016:04, the radar truck had been stationary. Between 2016:04 and 2017:05, data were collected while the radar truck was moving eastward. From 2017:05 until the last scan at 2018:36, the radar truck was again stationary. After 2017:05, the tornado vortex tracked along a path that was oriented approximately normal to the line of sight of the radar because the road was oriented roughly in the northeast–southwest direction rather than in the east–west direction, as it had been earlier (cf. Fig. 4 in Part I); it is possible that the tornado

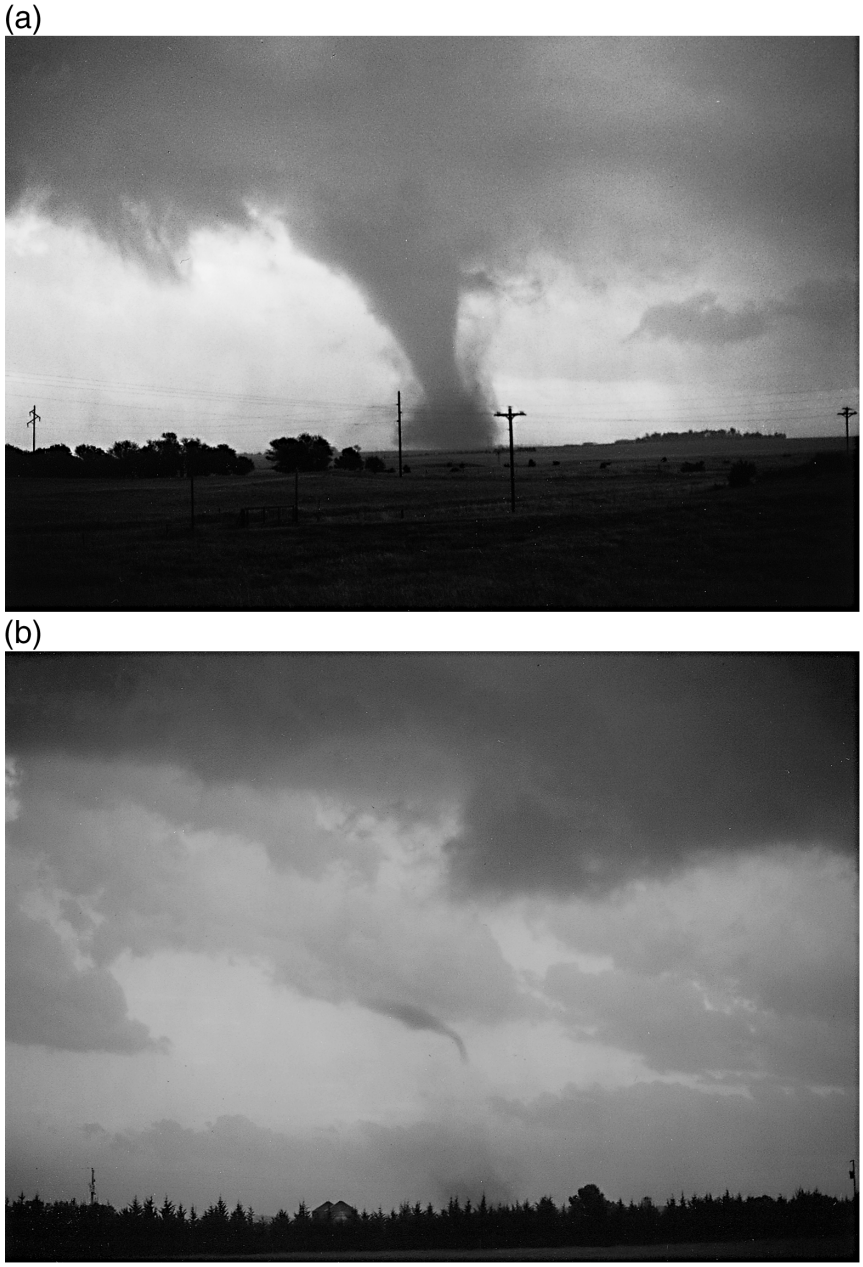

FIG. 2. Photographs of the tornado during (a) the mature stage (approximately 2017 CDT) and (b) the shrinking stage (approximately 2019 CDT), looking to the south-southwest and south-southeast, respectively, from U.S. Highway 20, 11.4 km and 10 km west, respectively, of Bassett, NE (see Fig. 4 in Part I) (photographs copyright H. Bluestein).

also changed direction slightly, but, lacking a damage survey, it is not possible to confirm this. When the tornado was most intense (after 2017:05) (Fig. 2a), the track was, as best can be determined from the Doppler radar data, a straight line.

The radar-relative track of the tornado vortex was also determined objectively using the techniques of Lee and Marks (2000); the objectively determined radar-relative track (not shown) was not significantly different from the subjectively determined track. After the tornado had dissipated as a dust whirl just to our east-southeast (Fig. 2b), another tornado formed to the northeast (but the radar team was unable to catch up to it and collect data until after it had dissipated).

At each data point in the vortex track seen in Fig. 1, a subjective estimate of the maximum horizontal shear in the Doppler velocity and the radius of maximum wind (RMW; one-half the distance between the Doppler wind

TABLE 1. Maximum Doppler shear, represented by the difference between extrema in Doppler velocity and RMW, estimated as one-half the distance between the Doppler velocity extrema, as a function of time (where XX and YY are given in min and s, respectively). (cf. Fig. 1 for the reference to the tornado track).

Time (20XX : YY CDT)	Maximum Doppler "shear" (m s^{-1})	RMW (m)	Vorticity (s^{-1})
2009 : 54	20	100	0.2
2010 : 28	29	75*/200	0.39*/0.15
2011 : 08	27	150	0.18
2011 : 51	34	150	0.22
2012 : 35	44	200	0.22
2013 : 29	61	200	0.3
2014 : 04	60	250	0.24
2014 : 42	63	250	0.26
2015 : 15	60	150	0.4
2015 : 53	63	200	0.32
2016 : 04	60	150	0.4
2016 : 23	68	150	0.46
2016 : 52	64	150	0.42
2017 : 05	75	125	0.6
2017 : 19	86	125	0.68
2017 : 33	89	100	0.9
2017 : 47	89	100	0.9
2018 : 02	94	100	0.94
2018 : 12	80	100	0.8
2018 : 25	75	125	0.6
2018 : 36	70	125	0.56

* The quantities shown are for the swirl in the radar echo only.

extrema) based on the Doppler velocity field were computed (Table 1). It is seen that the Doppler shear increased from only 20 m s^{-1} across the centers of extrema in the Doppler velocity field at 2009:54 to 94 m s^{-1} at 2018:02. The vorticity of the tornado could therefore have been as high as 0.9 s^{-1} (twice the change in Doppler velocity across the extremum couplet/twice the RMW). The mature tornado, within a minute or so of this time, is seen in Fig. 2a. Subsequently, the Doppler shear dropped to 70 m s^{-1}, which is still relatively high, even though the tornado condensation funnel was shrinking and disappearing (Fig. 2b), undergoing a process known colloquially as "roping out." The estimate of Doppler shear during the time the radar truck was moving may be in slight error owing to the motion of the observing platform (through errors in the pointing angle, etc.), but not significantly so, because the motion of the tornado had a substantial component normal to the line of sight of the radar.

Early on, the RMW was on the order of a few hundred meters, grew to 250 m, but after 2016:04 decreased to 100 m when the tornado was most intense. During the shrinking stage, the RMW was still only 125 m, which is relatively small. Thus, while the condensation funnel of the tornado was shrinking and disappearing, the narrowing of the condensation funnel was a misleading indicator of tornado intensity; in fact, the width of the tornado vortex near the ground was increasing slightly and the strength of the vortex remained relatively intense. The apparent wobbling of the tornado track after 2014:42, noted earlier, coincided with a time when the estimated RMW was sometimes relatively high (200–250 m); therefore some of the wobbling might be a result of errors in locating the center of the vortex when it was relatively wide and devoid of scatterers.

3. Analysis of the Doppler wind data: The GBVTD technique

In order to estimate the components of the wind field normal to the beam of the UMass radar and to separate the axisymmetric components of the wind from their angular harmonics, we applied the GBVTD technique of Lee et al. (1999) to sector scan data from 2012:35 through 2018:36 (cf. Fig. 1 and Table 1). The GBVTD technique is a modification to a fixed coordinate system of the velocity track display (VTD) technique, devised by Lee et al. (1994) to deduce properties of the primary circulation of tropical cyclones based on airborne Doppler radar data. The GBVTD and VTD techniques are inspired by the velocity-azimuth display (VAD) developed by Lhermitte and Atlas (1962).

It is assumed that a circularly symmetric vortex containing azimuthal (tangential) and radial components exists, along with higher-order angular harmonics of each wind component. Once the center of the vortex has been located objectively using the simplex method of Lee and Marks (2000), a truncated Fourier series of the azimuthal and radial wind components around the vortex center is fitted to the Doppler wind observations. In order to be able to determine the wind components and their harmonics, it is assumed that the asymmetric radial wind components are small in comparison to the corresponding azimuthal wind components (Lee et al. 1994); otherwise, the set of equations that must be solved to compute the wind components would be underdetermined. In tornadoes we expect that this simplifying assumption is usually a good one, except in some tornadoes very close to the ground, especially in high-swirl vortices (cf. Lewellen et al. 2000), where the asymmetric radial wind component is on the order of the azimuthal wind component (the axisymmetric radial wind component, however, which should be present in the inflow layer of most tornadoes, is not a problem). Efforts to separate the azimuthal wind component from the asymmetric radial wind component are underway by the second author; a discussion of the technique is beyond the scope of this paper.

In our application of the GBVTD technique to the W-band radar dataset, we neglect changes in height of the data over the small area probed by the radar, so that in effect we are treating low-elevation-angle data as constant-elevation data. The GBVTD technique works best when the aspect ratio [radius of the tornado-vortex core (region over which the vorticity is approximately constant)/distance from the center of the tornado to the radar] is low, that is, when the tornado is far enough away that all radar beams in the sector scan are nearly

parallel to each other. When the core radius is on the order of 100–200 m, tornadoes 1–2 km in range or greater are characterized by low aspect ratios. It is noted that this low aspect ratio criterion is yet another reason that data should not be collected in tornadoes at too close a range. [When the radar is located at the center of the vortex, the geometrical relationship between the components of the wind field and the Doppler wind field is identical to that of the VAD technique (Browning and Wexler 1968); for obvious reasons, however, the authors do not recommend collecting VAD data in tornadoes.]

Deductions about the nature of the tornado vortex based upon the azimuthally averaged radial and azimuthal winds determined from the GBVTD technique must be viewed with some caution. As already noted, if the magnitude of the asymmetric part of the radial wind component is not much less than that of the azimuthal wind component, then the results of the GBVTD could be in error. In addition, if the center of the vortex is not located accurately, the retrieved wind field will be in error (Lee and Marks 2000), especially if the vortex is highly asymmetric. In an axisymmetric vortex, the magnitude of the GBVTD-retrieved maximum azimuthal wind component decreases and the RMW (henceforth we will refer to the distance from the center of the vortex to the radius of the maximum *azimuthally averaged azimuthal wind component* as the RMW) increases as the error in the vortex center increases. A false wavenumber-1 asymmetry is also introduced: The maximum in wavenumber 1 is located in the opposite direction of the error-displaced center, and the magnitude of the wavenumber-1 error increases with increased displacement error.

When the radar-echo field has broad gaps in it, as it did early in the life of the 5 June 1999 tornado, some additional error could be introduced. From experience with idealized analytical wind fields, it has been shown that the maximum wavenumber resolved varies with the angular data gap: For gaps of 30°, 60°, 90°, and 180°, the maximum wavenumbers resolved are 3, 2, 1, and 0, respectively (data provdided by W.-C. Lee 2002).

Finally, centrifuging of scatterers radially outward (Dowell et al. 2001) could add a positive bias to the radial component of the wind field. The best retrievals of the wind field in the tornado are most likely those for which there is good temporal continuity and for which there is dynamical consistency with theoretical vortex behavior and other observations.

4. The structure of the tornado vortex

a. Azimuthal and radial wind profiles

The maximum azimuthally averaged azimuthal wind component approximately doubled from 14.5 m s^{-1} at 2012:35, to 30 m s^{-1} at 2017:47, and then diminished to 21.5 m s^{-1} at the time the tornado disappeared during the shrinking stage (Fig. 3). Coincident with the increase

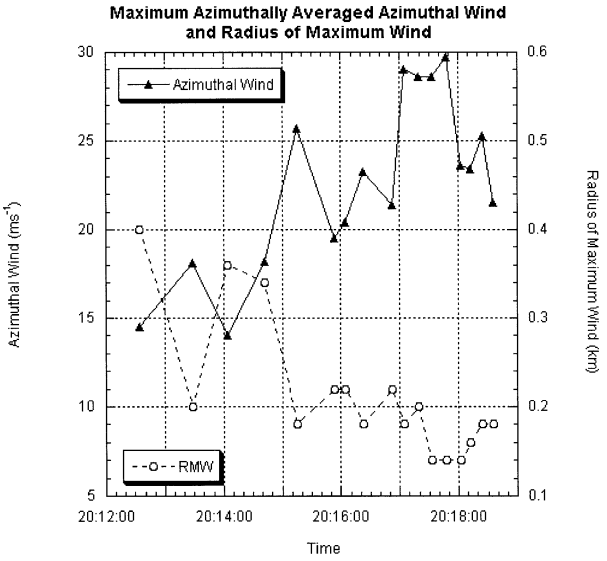

FIG. 3. Maximum azimuthally averaged azimuthal (tangential) wind component (solid line connected by solid triangles that represent the data points; scale at left) and the radial distance, from the assumed center of the tornado to the location of the maximum azimuthally averaged azimuthal wind component (RMW) (dashed line connected by open circles that represent the data points; scale at right), estimated from GBVTD analyses (cf. Fig. 4) as a function of time (CDT). At early times, when the radial variation in azimuthally averaged azimuthal wind component was relatively flat, the uncertainty in the location of the RMW is enhanced.

in maximum mean azimuthal wind speed, the RMW decreased from around 400 to 140 m (the RMW may have been even less than 140 m at times, but it cannot be confirmed because apparently there were not enough highly reflective scatterers at distances from the vortex center of around 100 m or less); subsequently, as the maximum mean azimuthal wind speed decreased, the RMW increased to 180 m. Thus, the time-dependent behavior of the tornado vortex while it intensified and while it dissipated is consistent with a ''spinning up'' of the vortex as its core[1] contracted and a ''spinning down'' of the vortex as its core expanded, in qualitative (but not quantitative) accord with the conservation of angular momentum in a frictionless fluid.

The reader is directed to Fig. 4 for the following discussion, which is valid for the time period after 2015:53, when application of the GBVTD technique was possible (the GBVTD technique was not applied to the data collected while the tornado was forming, as documented in Part I, owing to gaps in the data coverage). The azimuthally averaged azimuthal wind component generally increased approximately linearly with distance from the vortex center, about 20–40 m within the RMW. At a very small distance from the vortex center (within 100 m of the center), however, there were not enough

[1] The core is the region within the RMW where the vorticity is approximately constant; in a combined Rankine vortex the core extends outward to the RMW exactly.

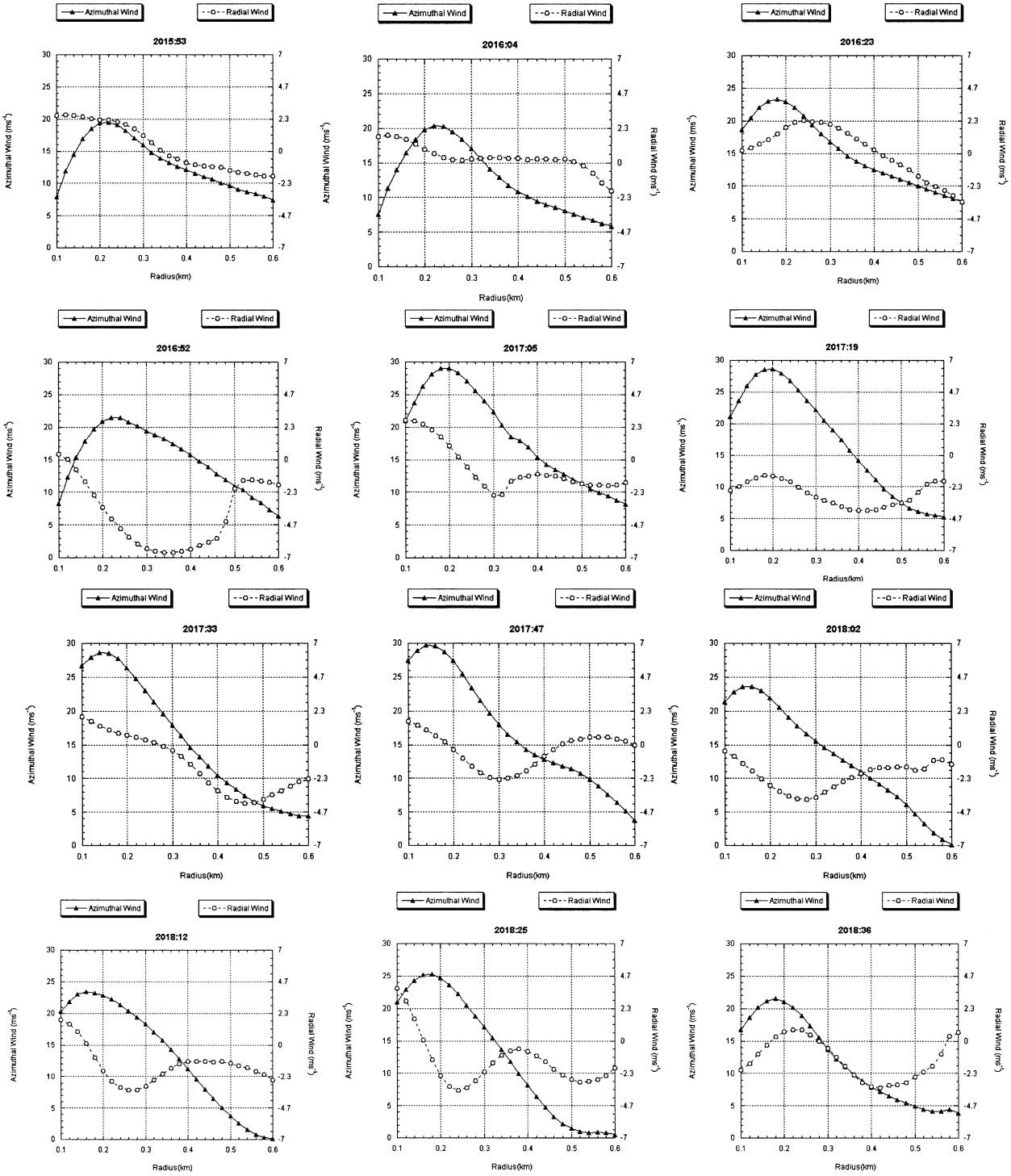

FIG. 4. Azimuthally averaged azimuthal wind component (wavenumber 0) (solid line connected by solid triangles that represent the data points; scale is to the left in each panel) and azimuthally averaged radial wind component (dashed line connected by open circles that represent the data points; scale is to the right in each panel) as a function of distance from the assumed center of the tornado, estimated by the GBVTD technique during the period from 2015:53 to 2018:36 CDT.

scatterers to determine the variation of wind with distance from the center. Beyond the RMW, the azimuthal wind dropped off relatively rapidly at first, and decreasingly rapidly at greater distance from the center. [The reader is reminded that the maximum azimuthally averaged azimuthal wind speeds indicated in Fig. 4 (~25–30 m s^{-1}) are less than what one would expect in anything but a minimal tornado; the *total* wind speeds, which also include the asymmetric components to be discussed subsequently, are much higher (~60–70 m s^{-1}).] The radial profile of the azimuthally averaged azimuthal wind component was qualitatively similar to that of a Rankine combined vortex, that is, a vortex composed of an inner region of solid-body rotation surrounded by potential flow (Davies-Jones 1986). Prior to 2015:53, however, before the tornado had formed, the azimuthally averaged azimuthal wind profile did not exhibit a well-defined RMW (not shown). A broader maximum about 200–250 m wide (not shown) may have been an artifact, since at the earlier times the distribution of scatterers about the center of the vortex was less uniform and did not completely encircle the vortex center.

After 2016:52, the radial wind component, with a few exceptions (e.g., at 2017:19 and 2018:36), in general decreased with increasing radius until approximately 100–250 m beyond the RMW. When the radial wind component decreased with radius about the RMW, it may be inferred that there was convergence, and, if the convergence was representative of the near-surface layer, rising motion above.

Also after 2016:52, the range at which the radial wind component dropped from positive (indicative of radial outflow) to negative values (indicative of radial inflow) was frequently near or just beyond the radius of maximum wind (exceptions were at 2017:19, 2018:02, and 2018:36). Very early on, at 2012:35, there was radial inflow out to near the RMW, and at 2013:29 there was radial inflow at close range (not shown).

The radial profiles of the azimuthally averaged radial wind component when the tornado was most intense (from 2017:05 to 2017:47; Fig. 5) are consistent with the structure of a two-celled vortex [cf. Figs. 6 and 10 in Rotunno (1984)]: divergence in the radial wind at the center of the vortex (indicated by positive radial velocity near the center), if representative of the near-surface layer, is associated with sinking motion above, and, around the RMW, the azimuthally averaged radial wind is convergent (radial wind component decreases with distance from the center of the vortex and may even become negative) and is associated with rising motion. (In the individual radial profiles in Fig. 4, positive radial velocity near the center dropped below zero within the RMW in seven cases; it fell below zero in three cases; in two cases the radial velocity was not positive near the center.) It is possible that there is some contamination of the azimuthally averaged radial component of the wind by particles centrifuged radially outward by

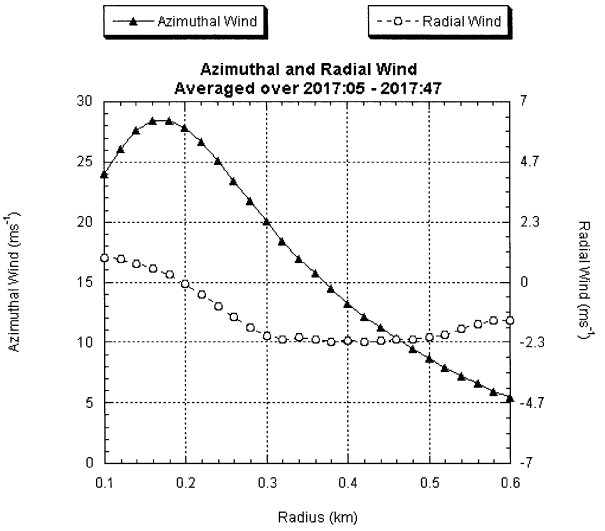

FIG. 5. As in Fig. 4, but for data averaged over the period from 2017:05 to 2017:47 CDT, when the tornado was most intense.

the tornado (Dowell et al. 2001). The radial motion (Fig. 4) was often positive only nearest the center of the vortex, within the RMW; one would expect that most of the significant centrifuging should take place close to the RMW, but on its near side, where the radius of curvature of parcel trajectories is relatively small; that is, the maximum centrifugal accelerations should be experienced at locations of *both* relatively high azimuthal wind speeds and relatively low distances from the vortex center. Knowledge of particle sizes is necessary to determine quantitatively whether or not there was a significant bias in the radial wind speed estimates.

In Fig. 3 it is seen that most of the time the RMW and maximum mean azimuthal wind were negatively correlated not only for the overall life of the tornado (minutes) but also on shorter timescales (tens of seconds). In particular, the correlation was negative during 11, positive during 1, and indeterminate during 5 time periods. During the time period when the mean azimuthal winds were the greatest (2017:33–2018:02), however, the RMW remained constant (''clipped'') at 140 m, mainly because there were not enough scatterers closer to the vortex center to determine if the RMW were closer in. It is not known whether or not the oscillations in the RMW and the maximum mean azimuthal wind on time periods of tens of seconds are significant or not, owing to aliasing and to errors resulting in applying the GBVTD technique. If the oscillations are indeed significant, they could represent a dynamical oscillation, perhaps as a result of inertial stability. The period of the oscillation decreases with tornado intensity from about 100 s early on to 30 s just before the tornado was most intense; thus, the period of oscillation is inversely related to the intensity (as measured by either the maximum wind speed or vorticity) of the tornado.

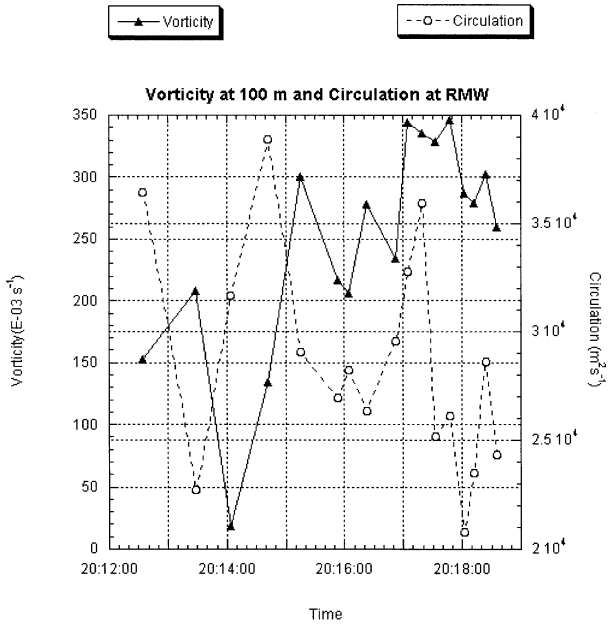

FIG. 6. Vorticity 100 m from the tornado center (10^{-3} s^{-1}) and circulation (m^2 s^{-1}) at the RMW as a function of time (CDT). Circulation and vorticity are computed from the azimuthally averaged azimuthal wind speed.

It was not possible to correlate damage with the estimates of wind speed to verify Fujita-scale estimates. Since the tornado occurred mostly over open country, a damage survey was not conducted. Because the translational motion of the tornado was only around 8–12 m s^{-1} (cf. the successive position of the vortex signatures in Fig. 1), maximum ground-relative wind speeds were at least 40 m s^{-1}, since the maximum azimuthally averaged azimuthal wind speed was 30 m s^{-1}. Maximum azimuthal wind speeds of 35–45 m s^{-1} were indicated in the GBVTD analyses of wavenumbers 0–3 to be discussed subsequently. Thus, we expect that the highest surface wind speeds may have been up to 55 m s^{-1}, which is within the F2 range (Fujita 1981).

b. Vorticity and retrieved perturbation pressure deficit

The vertical component of vorticity of the azimuthally averaged tornado vortex ($V/r + \partial V/\partial r$, where V is the azimuthally averaged azimuthal wind speed, and r is the distance from the center of the vortex) in its core, at 100 m, more than tripled from about 0.1 s^{-1} early on (before 2014:42) to around 0.35 s^{-1} between 2016:52 and 2017:47, and then decreased to approximately 0.25 s^{-1} as the tornado vortex was dissipating (Fig. 6). This increase of vorticity by a factor of 3.5 over a time period of approximately 170 s (from 2014:42 to 2017:33; see Fig. 6) is consistent with constant convergence ($-\delta$) of 7.4×10^{-3} s^{-1} alone acting on an air parcel passing into the vortex beginning at 2014:42 ($-\delta = 1/\Delta t \ln\zeta_f/\zeta_i$, where δ is the divergence acting over the time period Δt, and ζ_f and ζ_i are the final and initial vorticity, respectively). This estimate of convergence, however, is highly speculative because air parcels could pass through the tornado in less than 170 s or get caught in the tornado's secondary circulation and remain for an even longer time period. To interpret changes in circulation properly, one would have to follow parcels through the tornado, which is not possible to do with our dataset because, among other reasons, data are available only at one level.

If a circular, horizontal, fluid element having a radius equal to the RMW may be considered a material surface, then the decrease in the RMW from 340 m at 2014:42 to 140 m at 2017:33 (Fig. 3) is consistent with a constant convergence of 1.04×10^{-2} s^{-1} acting on an air parcel passing through the vortex after 2014:42 [$-\delta = 1/\Delta t$ ln(RMW$_f$/RMW$_i$), where RMW$_f$ and RMW$_i$ are the final and initial radii of maximum wind]. This estimate of convergence, like the former, is also highly speculative. The values of convergence acting on the vorticity of the tornado inferred via the two different methods are within approximately 25%–30% of each other.

The circulation at the RMW is another measure of the intensity of the tornado. The circulation at the RMW, although leading the trend in vorticity at 100 m before 2015:15 by 25 s or so, afterward was in phase with the trend in vorticity at 100 m (Fig. 6). However, the circulation at the RMW peaked at 2017:33 but decreased rapidly thereafter and even increased slightly as the tornado was dissipating. The circulation did not remain constant, while the vorticity at 100 m remained nearly constant (2017:05–2017:47) at its peak, because the RMW of the vortex decreased more rapidly than the maximum azimuthally averaged azimuthal wind speed increased. It thus appears that circulation at the RMW was not as good an indicator of the intensity of the tornado as the vorticity in its core because the latter followed the maximum azimuthal wind speed much better than the former (cf. Figs. 3 and 6). Since the circulation at the RMW represents the area-averaged vorticity for a fluid element enclosed by a circle of radius RMW, the vorticity at 100 m was not representative of the entire area covered by the RMW, as seen, for example, at 2017:47 in Fig. 7.

The variation of vorticity with distance from the center of the vortex is seen in Fig. 7. The vorticity decreased roughly linearly from its maximum value at 100 m to near zero, 100 m beyond the RMW. The vorticity in the core, outside of 100 m, was *not* uniform, as in a Rankine combined vortex. If the rate of increase of azimuthally averaged azimuthal wind component with distance from the center of the vortex had not fallen off near the RMW (Fig. 4; note the relatively smooth curvature in the azimuthal wind profiles near the RMW), then both the shear and curvature vorticity would have contributed to a higher value of vorticity inside the RMW and more of a solid-body-like rotation. It is likely that the smooth-

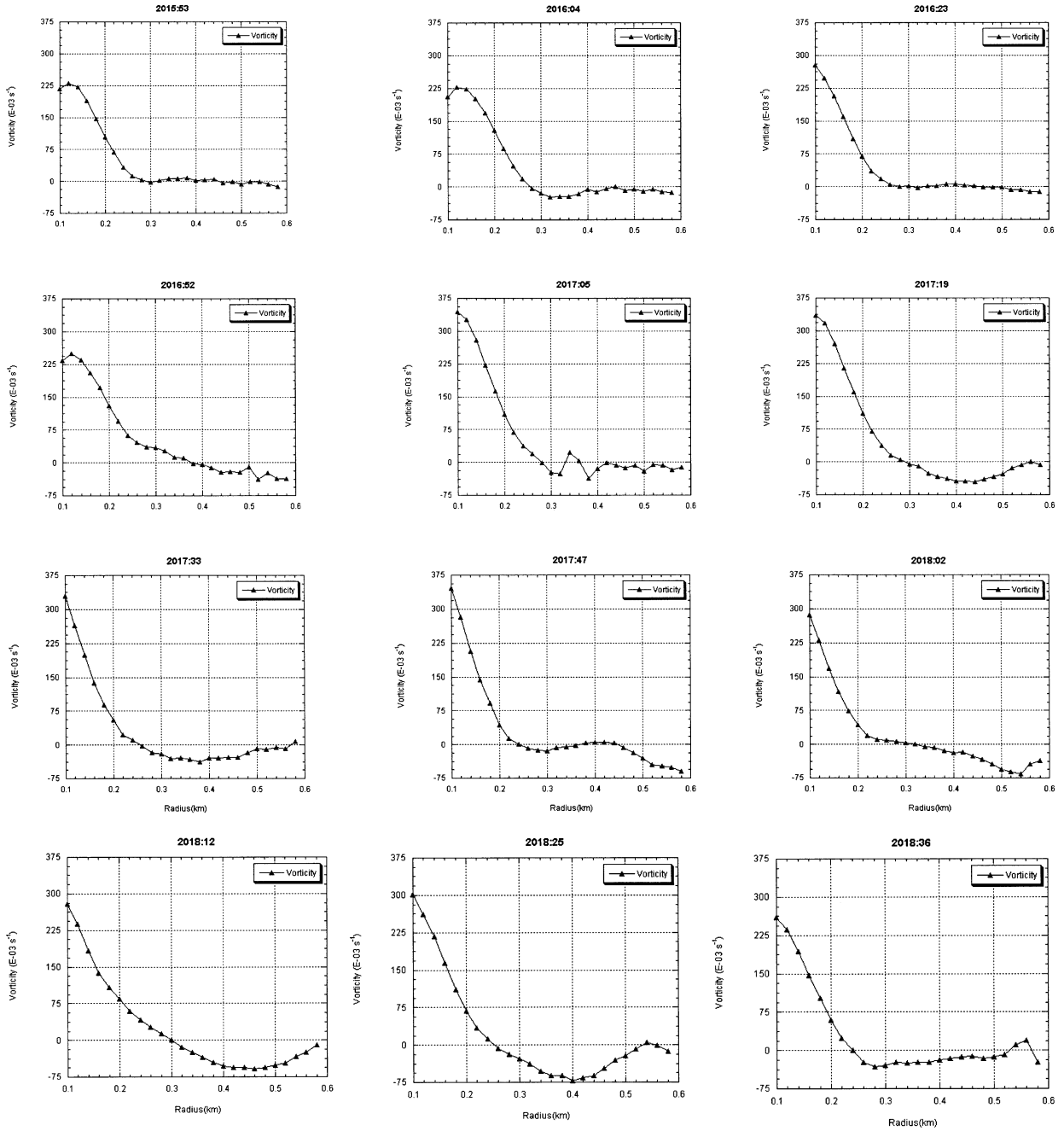

FIG. 7. Vorticity (10^{-3} s^{-1}) as a function of distance from the center of the tornado during the period from 2015:53 to 2018:36 CDT.

ness of the curve at the RMW is an artifact of the GBVTD technique, which filters out sharp gradients in the wind profile. An effect of an overly smoothed wind profile may be that, as noted in the previous paragraph, the circulation at the RMW was not the best indicator of tornado intensity. At some times there was a ring of weakly anticylonic vorticity outside the RMW, especially at 2018:12 and 2018:25, as the tornado was weakening.

The trends in both subjectively and objectively determined maximum wind and core radius were consistent. It has been noted (Table 1) that the maximum Doppler wind shear increased with time, reaching a maximum at 2018:02; thus, the maximum subjectively determined raw Doppler shear occurred only about 15 s after the maximum in objectively determined vorticity of the azimuthally averaged azimuthal wind (Fig. 6). The lowest subjectively estimated core radius after the tornado had formed was found between 2017:47 and 2018:12 (Table 1), a time period that includes the same

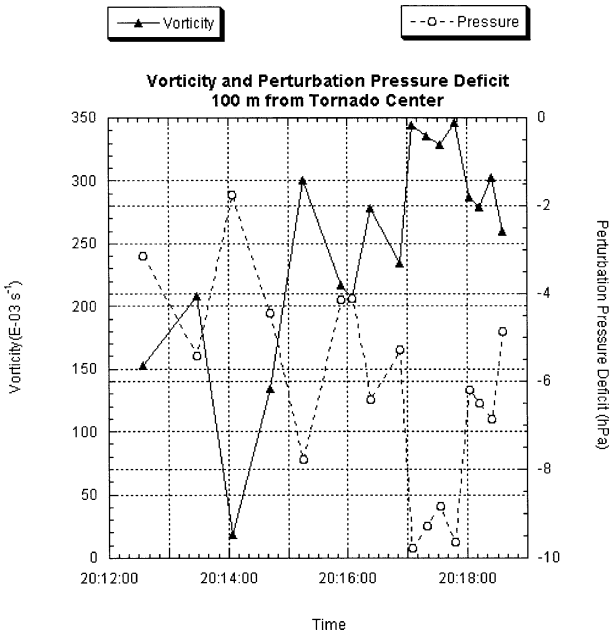

FIG. 8. Vorticity 100 m from the tornado center (10^{-3} s^{-1}) and estimate (assuming cyclostrophic balance) of the perturbation pressure deficit at the tornado center, relative to the perturbation pressure 600 m from the tornado center, as a function of time (CDT).

time span when the objectively determined RMW was at its minimum, that is, from 2017:47 to 2018:02 (Fig. 3).

At the time the tornado was most intense, Doppler shear topped 90 m s^{-1} over about 200 m (vorticity of approximately 2×90 m s^{-1}/200 m $= 0.9$ s^{-1}, which is more than twice the vorticity associated with the azimuthally averaged azimuthal wind). Since the GBVTD-determined estimates of vorticity discussed earlier are valid only for the circularly symmetric part of the azimuthal wind component and there were wind maxima associated with the asymmetric part of the azimuthal wind component (discussed in the following section), the winds associated with the asymmetric part of the wind must have made a significant contribution to the maximum wind speed and vorticity of the tornado. In addition, the smoothing effect on the wind profile of the GBVTD technique, as noted earlier, reduced the estimate of vorticity.

The perturbation pressure deficit (associated with the GBVTD analyses of the wind) at the center of the tornado, relative to the perturbation pressure outside the core, 600 m from the center (Fig. 7), was estimated by assuming the tornado was in cyclostrophic balance (Davies-Jones et al. 2001) (Fig. 8). The estimated pressure deficit and vorticity are, as expected, negatively correlated. Maximum retrieved pressure deficits were only around 10 hPa during the time period when the tornado was most intense. Such a pressure deficit is less than what has been seen in in situ measurements (Winn et al. 1999) and what has been found in numerical simulations of idealized tornado vortices (e.g., Rotunno 1984). Additional pressure deficits could be associated with a different vortex structure, deviations from cyclostrophic balance, or, to a lesser extent, to the asymmetric part of the wind field.

c. Asymmetric part of the tornado

Much of the structure of the azimuthal wind component of the tornado appeared to be in wavenumber-two disturbances (Fig. 9), as it was in the simulation of a laboratory tornado by Rotunno (1984; cf. his Fig. 9). For example, at most times there were two relative maxima in the azimuthal wind speed at opposite sides (with respect to the radar line of sight) of the tornado.

The reflectivity structure of the tornado varied very rapidly with time. A sequence of reflectivity images at approximately 10–15-s intervals exhibited significant temporal variations (Figs. 9 and 10); the tornado was apparently evolving rapidly in between scan times. Much of the time the eye (weak-echo hole near the center of the tornado) was elliptically shaped (Figs. 9 and 10), and in some scans spiral bands or other features having a wavenumber-two symmetry are seen. For example (Fig. 10), at 2016:52 and 2017:33 there were two narrow, *weak-echo* spiral bands [this structure is different from the spiral bands in hurricanes (e.g., Powell 1990) in that the latter are composed of relatively strong radar echoes]. Such spiral bands could be evidence of asymmetric radial wind components. At 2017:05 there is a prominent weak-echo notch on the far-side inner edge of the ''eyewall'' (outer edge of the echo-weak region; similar in appearance to the eyewall of a hurricane but at a much smaller scale). At 2017:19, the eye is no longer a simple oval-shaped weak-echo region, but instead there are two conjoined circular weak-echo holes. It is possible that the notch seen in the previous scan evolved into the second eye, but the reflectivity field changed too rapidly to confirm this speculation. At 2017:47, the eyewall has at least two weak-echo notches. Beginning at 2017:33, the leading edge of a narrow, weak-echo band seen in the lower right-hand side of Fig. 10 can be tracked as it rotated around the tornado until 2018:12. The eyewall enlarged slightly and became elongated, as the reflectivity of the scatterers in the tornado decreased rapidly between 2018:12 and 2018:36.

Much of the asymmetric eyewall structure seen in Fig. 10 is not an artifact caused by the motion of the radar truck since the structure was still very pronounced even after 2017:05, when the radar truck was stationary. Since the scans across the tornado took only a tiny fraction (~1–2 s) of each 10–15-s sector scan and since the translational motion of the tornado was around 10 m s^{-1} (cf. Fig. 1), any distortion of the reflectivity field would have been at the 10-m scale (if the tornado were moving normal to the line of sight of the radar) or less (if the tornado were moving at some angle across the line of sight of the radar), that is, not large enough in

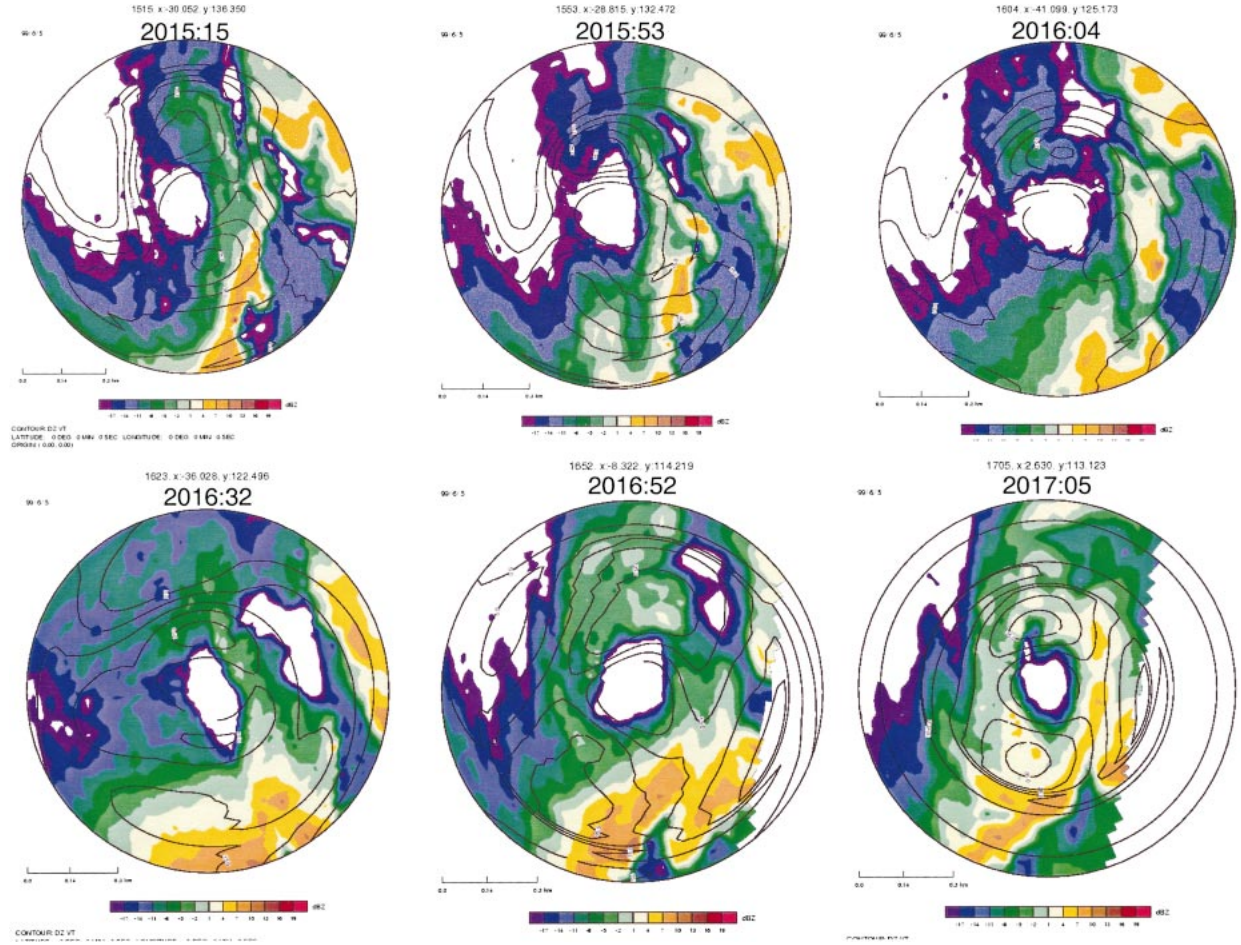

FIG. 9. GBVTD analysis of the Doppler radar velocity field, for the sum of wavenumbers 0–3 (solid contours in m s^{-1}) and the radar reflectivity field (color scales in dBZ), represented in polar coordinates from 2015:15 to 2018:36 CDT. The abscissa (ordinate) is aligned in the direction normal to (along) the radar beam when the beam passes through the center of the tornado vortex, as in Lee et al. (1999).

scale to be significant (in comparison with the ~200–300 m eye diameter).

The Doppler velocity structure of the tornado (Fig. 11) was also highly asymmetric, unlike that of a single Rankine combined vortex (Brown and Wood 1991). For example, at 2016:52 the maximum in inbound Doppler velocities (green areas) was broken up into two separate parts. At this time, the eyewall was elongated along the southwest-to-northeast direction (Fig. 10). At 2017:47 the Doppler velocities were also nonsymmetrically distributed across a line passing through the center of the vortex; however, at this time the eyewall was approximately square shaped rather than elliptically shaped (Fig. 10).

The prominence of the wavenumber-2 disturbances seen in Fig. 9 is now considered. Two waves in the wind field distributed around a Rankine combined vortex, according to an analysis by Lord Kelvin (Lamb 1945, 230–231; Rotunno 1984), should propagate at the angular phase speed of $\Omega/2$, where Ω is the solid-body rotation rate of the vortex core, or one-quarter of the vorticity of the core. Thus, the waves should retrograde with respect to the mean flow. These waves are like Rossby waves, but they owe their existence to radial gradients in the centrifugal force rather than in the Coriolis force. When vorticity 100 m from the center of the tornado peaked at 0.35 s^{-1} (Fig. 6), the angular phase speed of wavenumber-2 disturbances should have been 5.7° s^{-1}. Thus, in 12–14 s, the time between scans when the tornado was mature, each of the two waves should have moved 68°–80° around the tornado vortex, that is, about one-fifth of the way around. Although some of the wave locations would be aliased, it is likely that some scans would show the maxima in wavenumber two aligned at an angle approximately perpendicular to the radial direction.

In fact, most of the azimuthal wind maxima were oriented approximately along the radial direction or within about 10°–20° of it (Fig. 9). Even if the vorticity were approximately twice as strong (~1 s^{-1}) and the waves were completely aliased (they would have moved just under 180° between scans), one would still expect

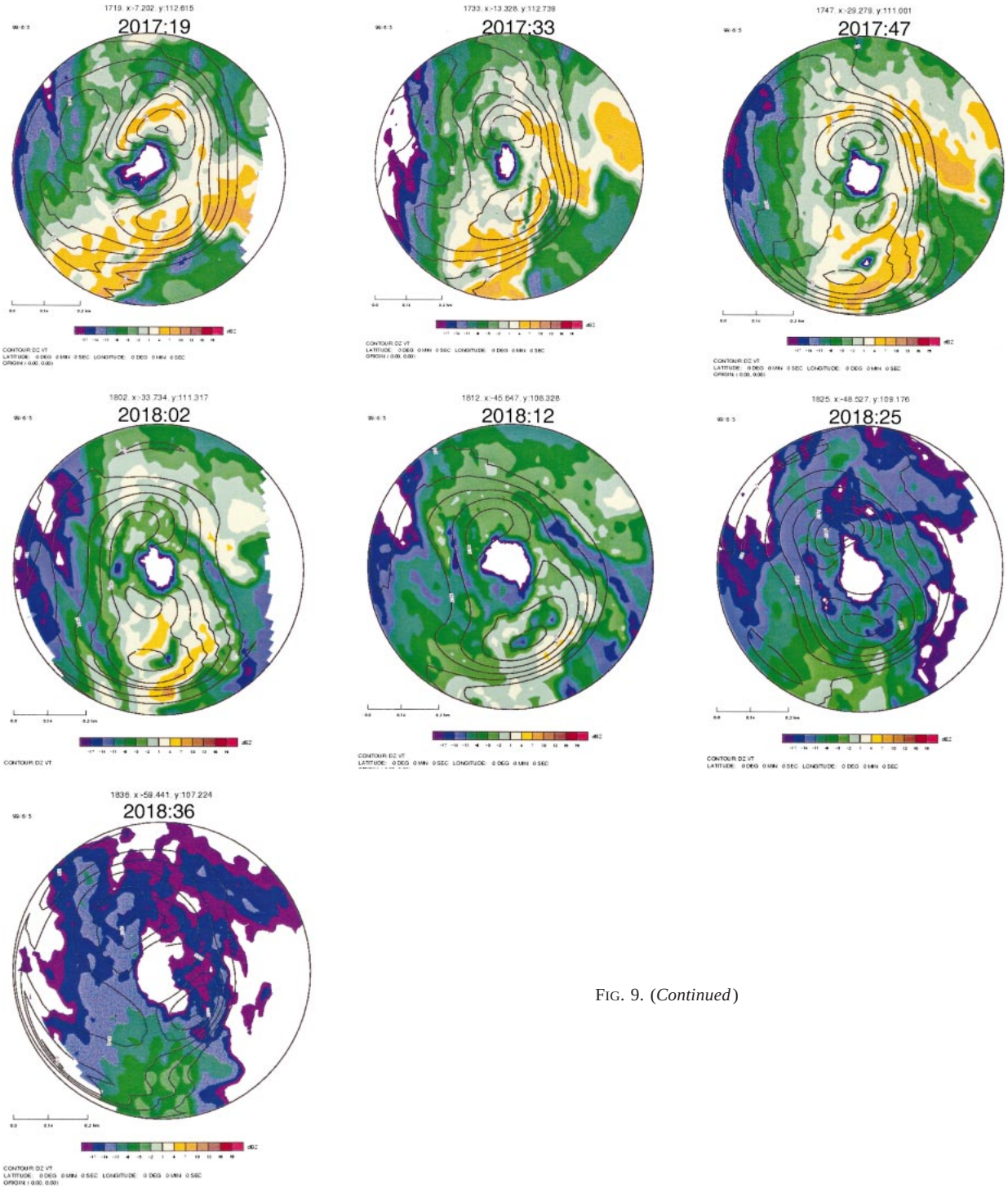

FIG. 9. (*Continued*)

to find, by chance, some maxima oriented approximately along the radial direction. With the exception of the 2016:52–2017:19 period, the speed maxima were aligned at a slight angle rotated in a counterclockwise angle from the line of sight. After 2015:15 the angle was around 10°; during the last part of the tornado's life, from 2018:25–2018:36, the angle was around 20°. Thus, it appears that the waves were quasi-standing; otherwise, we would have found the azimuthal wind speed maxima more randomly distributed about the center of the tornado. The major axis of the elliptically shaped tornado eyewall was also frequently, but not always, oriented within about 10°–20° of the line of sight. For example, at 2018:25 and 2018:36 it was ori-

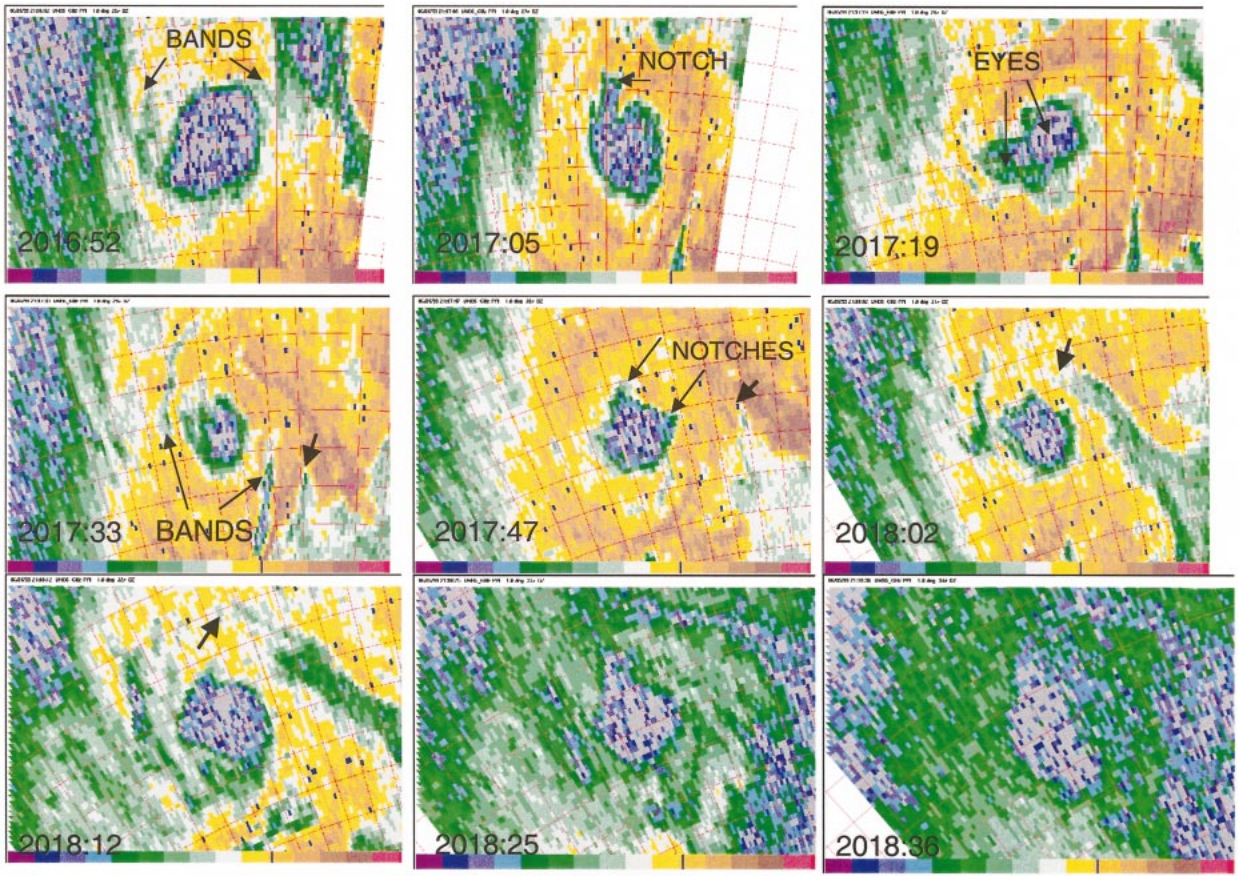

FIG. 10. Expanded view of the radar reflectivity factor (dBZ) field near the tornado, between 2016:52 and 2018:36 CDT. Color scales are shown under each panel. Red lines denote constant range markings every 100 m and constant-azimuth markings every 2.5° up to 2017:33 CDT, after which the constant-azimuth markings are shown every 2°. Echo-weak bands around the eye and notches along the outer edge of the eye are indicated at selected times. Bold arrows mark the leading edge of a narrow band of low reflectivity from 2017:33 to 2018:12 CDT.

ented about 20° counterclockwise from the line of sight, just as the line connecting the wavenumber-2 wind speed maxima was (Fig. 9); at 2016:52, it was oriented 20°–25° clockwise from the line of sight, just as the line connecting the wavenumber-2 wind speed maxima was (Fig. 9). There is thus independent evidence from the reflectivity field that the wavenumber-2 structure was not an artifact.

Further evidence was sought to find out whether the wavenumber-2 structure could have been an artifact caused by radar problems or errors in applying the GBVTD technique. It was first considered whether the wavenumber-two dominance could have been an artifact created by the sidelobe pattern of the radar antenna. How this could happen is as follows: If the radar truck were not leveled or if the terrain were higher in some direction other than that of the tornado, then backscatter from the ground at the range of the tornado might have resulted in a zero-velocity bias in the Doppler velocities at the range of the tornado if the backscattered signal were strong enough compared to that associated with the tornado. Thus, the across-the-beam wind velocities retrieved by the GBVTD technique might have been artificially enhanced. If this were the case, then the Doppler velocities inside the eye of the tornado would be nearly uniform and close to zero. Since the velocities were actually speckled inside the eye (Fig. 11), indicating that the radar signal was below the noise level, sidelobe contamination could not have been responsible for the wavenumber-2 dominance.

Independent evidence of the wavenumber-2 structure in data from another radar operating with a different field of view was sought by applying the GBVTD technique to data from the Doppler on Wheels 2 (DOW2) (DOW3 data were not reliable at the time of the tornado), a mobile X-band Doppler radar system (see Part I for more details about the DOW2 and DOW3) also deployed near Bassett, Nebraska, on 5 June 1999. At 2018:11 (cf. the 2018:12 panel in Fig. 9), a GBVTD analysis of the DOW2 data exhibited a wavenumber-2 structure (not shown) similar to the one seen in Fig. 9, except that the nearer of the two wind-speed maxima was weaker and rotated slightly to the west. This comparison must be interpreted with some caution, however;

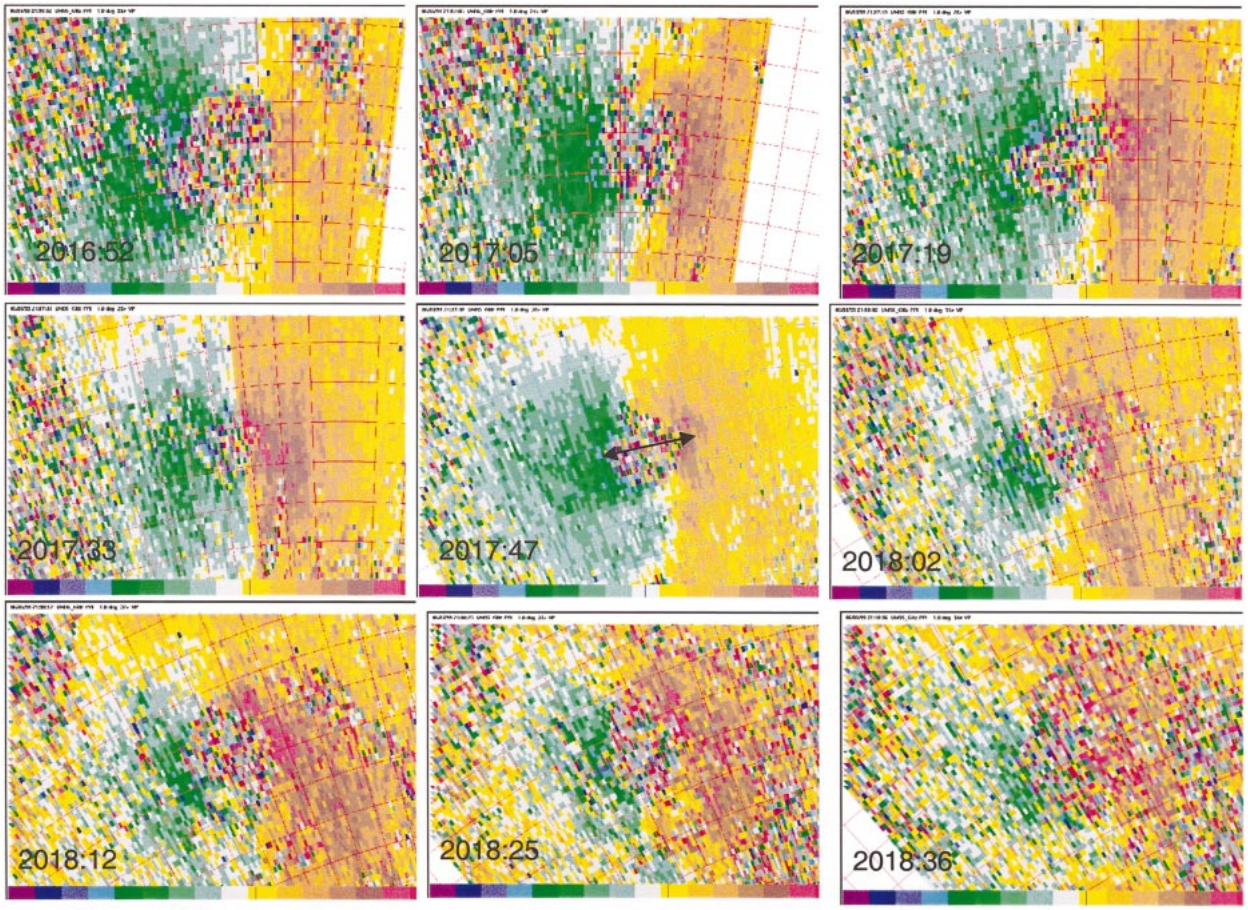

FIG. 11. As in Fig. 10, but for Doppler velocity (range and azimuth markings at 2017:47 CDT only are given in green rather than red). Doppler velocity color scale ranges from -60 m s^{-1} at the left to 50 m s^{-1} at the right at all times except at 2017:47 CDT, when the color scale ranges from -70 m s^{-1} at the left to 70 m s^{-1} at the right. The vortex signature at 2017:47 CDT (green–blue to brown–red) is pointed out by the line with arrows.

since DOW2 was farther away from the tornado, its spatial resolution was much less owing to its wider-beam antenna, the elevation angle was probably higher than that of the W-band radar system, and no effort was made to synchronize the clocks of the W-band radar and the DOW2 radar. It is tentatively concluded, therefore, that the quasi-stationary wavenumber-2 dominance seen in Fig. 9, if it is indeed an artifact, would likely have been a result of the GBVTD technique and not a radar problem.

It is possible that the elliptical shape of the eyewall and the asymmetric vortex structure were caused not entirely or at all by wave motion, but rather in part by the asymmetrical effects of surface shear stress related to the translation of the tornado vortex (Lewellen et al. 2000; cf. their Figs. 2 and 14). Lewellen et al. (2000) argued that the effect on surface stress would be more significant farther from the center of the vortex, where the relative magnitude of the translation speed to the azimuthal wind speed is greater. A result of this change in distribution of surface stress is that the swirl ratio would be lowered so that there are fewer secondary vortices and that one or two are stronger than the rest. It is not known, however, if or how translation speed could be responsible for stationary wavenumber-2 disturbances. Yamauchi et al. (2002) found, from a triple-Doppler analysis of a typhoon, that an elliptically shaped vortex could be the result of the superposition of a Rankine vortex and a field of pure deformation. It is speculated, then, that the asymmetry in the tornado could have been due to deformation.

d. Vortex structure during the shrinking stage

While the tornado was going through the shrinking stage, the RMW increased slightly from 140 to 180 m (Fig. 3), the maximum mean azimuthal wind speed decreased to about 22 m s^{-1} from its maximum of 30 m s^{-1} just under 60 s earlier. The maximum Doppler shear across the vortex signature on the last scan when the tornado was quickly disappearing (Table 1) was 70 m s^{-1}, which is still relatively high. These findings are in

accord with other observations that during the shrinking stage, some tornadoes can remain quite intense (e.g., Davies-Jones et al. 1978; Bluestein et al. 1993). A possible exception, to some extent, is the first tornado analyzed in the 8 June 1995 case by Dowell and Bluestein (2002), in which the width of the Doppler velocity signature decreased during the dissipation stage.

5. Accuracy of the GBVTD technique

Although the time tendencies of the GBVTD-derived parameters (maximum azimuthal wind speed, RMW, vorticity, etc.) and their interrelationships make physical sense, absolute values of the parameters must be viewed with caution. When the tornado was most intense, the RMW was 140 m (or less). On the other hand, from the raw Doppler velocities it was found that the minimum distance between the extrema of the vortex signature was around 200 m (Table 1). Therefore the core radius of the tornado, when it was most intense, was probably between 100 and 140 m.

A photograph of the tornado was analyzed to see if this estimate of core radius is consistent with the GBVTD analysis of the Doppler data. After photogrammetric analysis of the tornado photograph shown in Fig. 2a, using the range of the tornado determined from the Doppler vortex signature (2.2 km in Fig. 11), it was estimated that the width of the debris cloud near the ground was 175 m, the width of the condensation funnel near the debris cloud was 65 m, the width of the condensation funnel near cloud base was 175 m, and the height of cloud base was 440 m. The latter is quantitatively consistent with the lifting condensation level (LCL) of the sounding in Fig. 2 of Part I. However, it appears that the width of the debris cloud (175 m) was slightly less than the width of the core of the tornado (200–280 m). The photogrammetrically analyzed width of 175 m is less than most of the widths estimated photogrammetrically in earlier studies (e.g., see Table 3 in Bluestein et al. 1993). It is believed, however, that the core radius measurements based on the GBVTD analyses may be too high by about 45–50 m because it is unlikely that the debris cloud was narrower than the core radius, unless the radius of maximum upward motion was located within the RMW. Using idealized analytical wind fields, Lee and Marks (2000) found that an estimate of the RMW increases with an increase in error of the location of the vortex center, but that the magnitude of the error is very small. Another possibility, as already noted, which is more likely, is that because there were apparently few radar-reflective scatterers inside the tornado core, the RMW was actually less than 140 m; based on the photogrammetric analysis of the debris cloud, it is possible the RMW could have been as low as 85–90 m.

The sensitivity of the retrieved wind fields to the location of the vortex center was tested at 2017:47, when the data coverage was very good and the tornado most intense, by displacing the center ±25 m in the direction normal to the line of sight of the radar and ±25 m in the direction along the line of sight of the radar. It is seen that the mean azimuthal wind component profile is not very sensitive to displacements of the vortex center (Fig. 12), whereas the mean radial wind component profile is quantitatively sensitive, but not qualitatively sensitive; that is, the radial wind component profiles all look similar, but the differences among radial wind components can vary by as much as 50% (e.g., 1.5 m s^{-1} at 280 m), while the radial gradients are of the same sign. The magnitudes of the mean radial wind components must therefore be viewed with extra caution. For example, the distance from the center of the vortex at which the radial wind component first goes to zero varies from near the RMW to 60 m beyond the RMW. Some of the displacement of the first zero in radial velocity beyond the RMW, however, could be due to centrifuging (Dowell et al. 2001). The location of the RMW at this time, however, is not sensitive to the location of the vortex center.

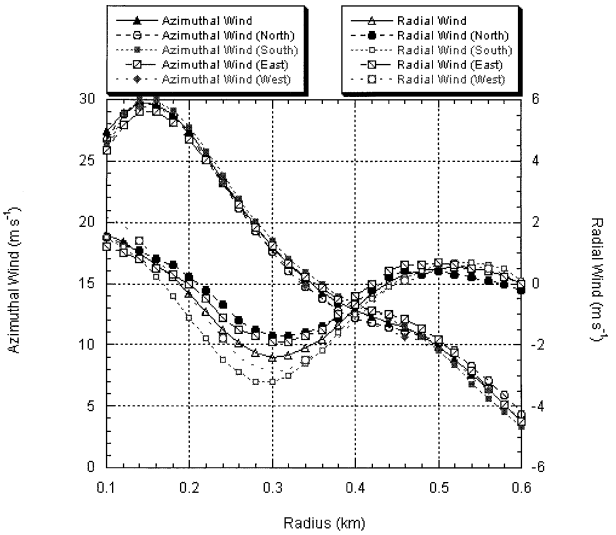

FIG. 12. Sensitivity of the radial profiles of the azimuthally averaged azimuthal wind component and radial wind component to changes in the location of the tornado-vortex center at 2017:47 CDT by ±25 m (''north'' and ''south,'' respectively) in the direction along the line of sight (radials) of the radar and ±25 m (''east'' and ''west,'' respectively) in the direction normal to the line of sight of the radar (at constant range).

The mean standard deviation of the wavenumber-1 component of the azimuthal wind for all times (not shown) is about 3–4 times that of the mean azimuthal wind component and of the mean radial wind component. The wavenumber-1 wind components must therefore also be viewed with extra caution (Lee and Marks 2000).

6. Summary and discussion

The near-surface wind field of the 5 June 1999 tornado vortex, for most of its lifetime, was heavily weight-

ed by wavenumber-2 disturbances in the azimuthal wind component. There have been many studies of the dynamic stability of tornado-like vortices (Snow 1978; Rotunno 1978, 1984; Gall 1983, 1985; Walko and Gall 1984; Staley and Gall 1979, 1984; Nolan and Farrell 1999). In general, instabilities are related to the radial gradient of vorticity of the azimuthally averaged azimuthal component of the wind. Finding sharp radial gradients in nature is probably difficult because the secondary circulation in a vortex acts to reduce the radial gradients (Rotunno 1984) originally responsible for the instability. Radial shear of vertical velocity in axisymmetric vortices acts to destabilize vortices that would otherwise be stable. The number of smaller-scale disturbances in a vortex is a monotonic function of the swirl ratio (Walko and Gall 1984); such behavior has been observed in laboratory simulations (Davies-Jones et al. 2001). In our case, it was not possible to estimate the swirl ratio because data were collected at only one level. Since the wavenumber-2 disturbances did not appear to translate around the mean vortex, it is more likely that they, if they are indeed real, may, alternatively, be a result of vortex translation and surface stress and/or deformation. More case studies that relate the dominant wavenumber contribution to translation speed might resolve this issue. In addition, the GBVTD technique needs to be examined further for cases when the asymmetric component of the radial wind is comparable to the azimuthal wind so that artifacts are not produced.

Other significant findings were that the core radius of the tornado, as measured by the RMW, decreased as the tornado intensified, as would be expected if convergence were acting on it, and increased slightly as it weakened. In the shrinking stage the tornado remained relatively intense and wide, even though the condensation funnel narrowed and disappeared. It is speculated that relatively dry air must have been entrained into the tornado vortex during the shrinking stage, so that the narrowing of the funnel was not a result of a significant increase in pressure. A photograph of a tornado funnel disappearing aloft during the shrinking stage in another storm has been interpreted as dry air from aloft subsiding and being entrained into the vortex (Bluestein et al. 1988).

The 5 June 1999 tornado dataset is the only one collected by the W-band radar so far in which the properties of a tornado vortex were documented during its entire life history. The properties of many other tornado vortices based on a GBVTD analysis of radar data, compiled into a climatology, need to be documented to see the range of behavior exhibited in nature of different tornadoes. Scans at a succession of different levels need to be made at the sacrifice of temporal continuity, so that the swirl ratio can be estimated (Lee and Wurman 2001), because much of the behavior of a tornado vortex is controlled by it (Davies-Jones et al. 2001). It is also important that radar data be collected that document the overall storm behavior while the W-band radar focuses on the tornado. In the past, efforts to coordinate with other mobile X-band radars were not generally successful. Future continued efforts should include mobile X-band or C-band scans of the entire storm.

Finally, the issue of how tornado intensity should be measured is briefly addressed. Tornado ''intensity'' may be measured by the maximum ground-relative wind speed at the surface, which is actually responsible for the relative amount of damage inflicted, or by the maximum tornado-relative wind speed at the surface, which in a Rankine combined vortex is proportional to the vorticity and the core radius, or to the circulation at the RMW. In the 5 June 1999 case, damage estimates were not available. However, radar-derived estimates of the maximum wind speed as a function of time were obtained. Since the maximum ground-relative wind speed is dependent not only on the actual azimuthal wind speed but also on the translation speed of the tornado vortex, it seems that *any damage estimate or ground relative Doppler radar–derived wind speed does not reflect the true intensity of the tornado itself*. It is suggested that vorticity of the core of a tornado, computed at the same radius within the RMW, might be the best way to characterize the intensity of a tornado, since within an idealized core there is uniform vorticity, and *the processes that control the intensity of a tornado should not depend on the reference frame.* In the 5 June 1999 case, however, a uniform vorticity distribution within the core was not apparent, as noted, probably owing to a lack of reflective scatterers close to the center of the tornado vortex and to smoothing inherent in the GBVTD algorithms. Circulation at the RMW did not appear to be a good measure of the intensity of the 5 June 1999 tornado, owing to variations in vorticity in the core, within the RMW. Any effort to relate parent-storm or environmental characteristics to tornado intensity should therefore involve vorticity computed within the core, but as close to the center of the tornado as possible. An assessment of the potential destructive power from a tornado, on the other hand, should include not only its vorticity, but also its translational speed. Thus, while using the GBVTD technique to assess the damage potential of a tornado, one should also include its translation speed.

Acknowledgments. We are indebted to the following OU graduate students for the assistance we received during the field experiment in which the data for this study were collected: Greg Lehmiller, Peter Leptuch, and David Dowell. They shared the driving and assisted in making real-time decisions. Erik Rasmussen (NSSL/CIMMS) provided nowcasting support. Josh Wurman (OU) and Jerry Straka (OU) also provided real-time information; the former also graciously shared his team's DOW data, which David Dowell provided. Mark Laufersweiler (OU) assisted with computer-related issues. We are indebted to John Snow, Rich Rotunno, David Nolan, and Kerry Emanuel for discussions about

vortex dynamics. This project was funded by NSF Grants ATM-9612674 and -9912097 to OU and by ATM-9616730 to the University of Massachusetts—Amherst. The first author was a visitor on sabbatical leave in the Mesoscale and Microscale Meteorology Division of the National Center for Atmospheric Research (NCAR) during the final part of this study.

REFERENCES

Bluestein, H. B., 1999: A history of storm-intercept field programs. *Wea. Forecasting,* **14,** 558–577.

——, and A. L. Pazmany, 2000: Observations of tornadoes and other convective phenomena with a mobile, 3-mm wavelength, Doppler radar: The spring 1999 field experiment. *Bull. Amer. Meteor. Soc.,* **81,** 2939–2951.

——, E. W. McCaul Jr., G. P. Byrd, and G. Woodall, 1988: The unusual dissipation of a tornado funnel. *Mon. Wea. Rev.,* **116,** 950–952.

——, W. P. Unruh, J. LaDue, H. Stein, and D. Speheger, 1993: Doppler radar wind spectra of supercell tornadoes. *Mon. Wea. Rev.,* **121,** 2200–2221.

——, A. L. Pazmany, J. C. Galloway, and R. E. McIntosh, 1995: Studies of the substructure of severe convective storms using a mobile 3-mm wavelength Doppler radar. *Bull. Amer. Meteor. Soc.,* **76,** 2155–2169.

——, S. G. Gaddy, D. C. Dowell, A. L. Pazmany, J. C. Galloway, R. E. McIntosh, and H. Stein, 1997a: Mobile, 3-mm wavelength, pulsed Doppler radar observations of substorm-scale vortices in a supercell. *Mon. Wea. Rev.,* **125,** 1046–1059.

——, W. P. Unruh, D. C. Dowell, T. A. Hutchinson, T. M. Crawford, A. C. Wood, and H. Stein, 1997b: Doppler radar analysis of the Northfield, Texas, tornado of 25 May 1994. *Mon. Wea. Rev.,* **125,** 212–230.

——, C. C. Weiss, and A. L. Pazmany, 2003: Mobile Doppler radar observations of a tornado in a supercell near Bassett, Nebraska, on 5 June 1999. Part I: Tornadogenesis. *Mon. Wea. Rev.,* **131,** 2954–2967.

Brown, R. A., and V. T. Wood, 1991: On the interpretation of single-Doppler velocity patterns within severe thunderstorms. *Wea. Forecasting,* **6,** 32–48.

Browning, K. A., and R. Wexler, 1968: The determination of kinematic properties of a wind field using Doppler radar. *J. Appl. Meteor.,* **7,** 105–113.

Davies-Jones, R. P., 1986: Tornado dynamics. *Thunderstorm Morphology and Dynamics,* E. Kessler, Ed., University of Oklahoma Press, 197–236.

——, D. W. Burgess, L. R. Lemon, and D. Purcell, 1978: Interpretation of surface marks and debris patterns from the 24 May 1973 Union City, Oklahoma tornado. *Mon. Wea. Rev.,* **106,** 12–21.

——, R. J. Trapp, and H. B. Bluestein, 2001: Tornadoes and tornadic storms. *Severe Convective Storms, Meteor. Monogr.,* No. 50, Amer. Meteor. Soc., 167–221.

Dowell, D. C., and H. B. Bluestein, 2002: The 8 June 1995 McLean, Texas, storm. Part II: Cyclic tornado formation, maintenance, and dissipation. *Mon. Wea. Rev.,* **130,** 2649–2670.

——, J. Wurman, and L. J. Wicker, 2001: Centrifuging of scatterers in tornadoes. Preprints, *30th Int. Conf. on Radar Meteorology,* Munich, Germany, Amer. Meteor. Soc., 307–309.

Fujita, T. T., 1981: Tornadoes and downbursts in the context of generalized planetary scales. *J. Atmos. Sci.,* **38,** 1511–1534.

Gall, R. L., 1983: A linear analysis of the multiple vortex phenomenon in simulated tornadoes. *J. Atmos. Sci.,* **40,** 2010–2024.

——, 1985: Linear dynamics of the multiple-vortex phenomenon in tornadoes. *J. Atmos. Sci.,* **42,** 761–772.

Lamb, H., 1945: *Hydrodynamics.* Dover, 738 pp.

Lee, W.-C., and F. D. Marks Jr., 2000: Tropical cyclone kinematic structure retrieved from single-Doppler radar observations. Part II: The GBVTD-simplex center finding algorithm. *Mon. Wea. Rev.,* **128,** 1925–1936.

——, and J. Wurman, 2001: Diagnosis of 3D wind structure of a tornado using VTD analysis. Preprints, *30th Int. Conf. on Radar Meteorology,* Munich, Germany, Amer. Meteor. Soc., 304–305.

——, F. D. Marks Jr., and R. E. Carbone, 1994: Velocity track display—A technique to extract real-time tropical cyclone circulations using a single airborne Doppler radar. *J. Atmos. Oceanic Technol.,* **11,** 337–356.

——, B. J.-D. Jou, P.-L. Chang, and S.-M. Deng, 1999: Tropical cyclone kinematic structure retrieved from single-Doppler radar observations. Part I: Interpretation of Doppler velocity patterns and the GBVTD technique. *Mon. Wea. Rev.,* **127,** 2419–2439.

Lewellen, D. C., W. S. Lewellen, and J. Xia, 2000: The influence of a local swirl ratio on tornado intensification near the surface. *J. Atmos. Sci.,* **57,** 527–544.

Lhermitte, R. M., and D. Atlas, 1962: Precipitation motion by pulse Doppler radar. *Proc. Ninth Weather Radar Conf.,* Kansas City, MO, Amer. Meteor. Soc., 218–223.

Nolan, D. S., and B. F. Farrell, 1999: Generalized stability analyses of asymmetric disturbances in one- and two-celled vortices maintained by radial inflow. *J. Atmos. Sci.,* **56,** 1282–1307.

Powell, M. D., 1990: Boundary layer structure and dynamics in outer hurricane rainbands. Part I: Mesoscale rainfall and kinematic structure. *Mon. Wea. Rev.,* **118,** 891–917.

Rotunno, R., 1978: A note on the stability of a cylindrical vortex sheet. *J. Fluid Mech.,* **87,** 761–771.

——, 1984: An investigation of a three-dimensional asymmetric vortex. *J. Atmos. Sci.,* **41,** 283–298.

Snow, J. T., 1978: On inertial instability as related to the multiple-vortex phenomenon. *J. Atmos. Sci.,* **35,** 1660–1677.

Staley, D. O., and R. L. Gall, 1979: Barotropic instability in a tornado vortex. *J. Atmos. Sci.,* **36,** 973–981.

——, and ——, 1984: Hydrodynamic instability of small eddies in a tornado vortex. *J. Atmos. Sci.,* **41,** 422–429.

Walko, R., and R. Gall, 1984: A two-dimensional linear stability analysis of the multiple vortex phenomenon. *J. Atmos. Sci.,* **41,** 3456–3471.

Winn, W. P., S. J. Hunyady, and G. D. Aulich, 1999: Pressure at the ground within and near a large tornado. *J. Geophys. Res.,* **104** (D18), 22 067–22 082.

Wurman, J., 2002: The multiple-vortex structure of a tornado. *Wea. Forecasting,* **17,** 473–505.

——, and S. Gill, 2000: Finescale radar observations of the Dimmitt, Texas (2 June 1995), tornado. *Mon. Wea. Rev.,* **128,** 2135–2164.

Yamauchi, H., O. Suzuki, and K. Akaeda, 2002: Asymmetry in wind field of Typhoon 0115 analyzed by triple Doppler radar observations. Preprints, *Int. Conf. on Mesoscale Convective Systems and Heavy Rainfall/Snowfall in East Asia,* Tokyo, Japan, Japan Science and Technology Corporation and Chinese Academy of Meteorological Sciences, 245–250.